Global Journal of Computer Science and Technology: E Network, Web & Security
Volume 18 Issue 1 Version 1.0 Year 2018
Type: Double Blind Peer Reviewed International Research Journal
Publisher: Global Journals
Online ISSN: 0975-4172 & Print ISSN: 0975-4350

Secured Audio Signal Transmission in 5G Compatible mmWave Massive MIMO FBMC System with Implementation of Audio-to-Image Transformation Aided Encryption Scheme

By Jinia Rahman, Joarder Jafor Sadique, Md. Sarwar Hossain & Shaikh Enayet Ullah
University of Rajshahi

Abstract- In this paper, we have made comprehensive study for the performance evaluation of mmWave massive MIMO FBMC wireless communication system. The 16×256 large MIMO antenna configured simulated system under investigation incorporates three modern channel coding (Turbo, LDPC and (3, 2) SPC, higher order digital modulation (256-QAM)) and various signal detection (Q-Less QR, Lattice Reduction(LR) based Zero-forcing(ZF), Lattice Reduction (LR) based ZF-SIC and Complex-valued LLL(CLLL) algorithm implemented ZF-SIC) schemes. An audio to image conversion aided chaos-based physical layer security scheme has also been implemented in such study. On considering transmission of encrypted audio signal in a hostile fading channel, it is noticeable from MATLAB based simulation study that the LDPC Channel encoded system is very much robust and effective in retrieving color image under utilization of Lattice Reduction(LR) based ZF-SIC signal detection and 16- QAM digital modulation techniques.

Keywords: MIMO-FBMC, chaos-based physical layer security, digital precoding, mmwave geometrical channel, SNR.

GJCST-E Classification: C.2.1, D.4.4

Strictly as per the compliance and regulations of:

© 2018. Jinia Rahman, Joarder Jafor Sadique, Md. Sarwar Hossain & Shaikh Enayet Ullah. This is a research/review paper, distributed under the terms of the Creative Commons Attribution-Noncommercial 3.0 Unported License http://creativecommons.org/licenses/by-nc/3.0/), permitting all non-commercial use, distribution, and reproduction inany medium, provided the original work is properly cited.

Secured Audio Signal Transmission in 5G Compatible mmWave Massive MIMO FBMC System with Implementation of Audio-to-Image Transformation Aided Encryption Scheme

Jinia Rahman [α], Joarder Jafor Sadique [σ], Md. Sarwar Hossain [ρ] & Shaikh Enayet Ullah [ω]

Abstract- In this paper, we have made comprehensive study for the performance evaluation of mmWave massive MIMO FBMC wireless communication system. The 16×256 large MIMO antenna configured simulated system under investigation incorporates three modern channel coding (Turbo, LDPC and (3, 2) SPC, higher order digital modulation (256-QAM)) and various signal detection (Q-Less QR, Lattice Reduction(LR) based Zero-forcing(ZF), Lattice Reduction (LR) based ZF-SIC and Complex-valued LLL(CLLL) algorithm implemented ZF-SIC) schemes. An audio to image conversion aided chaos-based physical layer security scheme has also been implemented in such study. On considering transmission of encrypted audio signal in a hostile fading channel, it is noticeable from MATLAB based simulation study that the LDPC Channel encoded system is very much robust and effective in retrieving color image under utilization of Lattice Reduction(LR) based ZF-SIC signal detection and 16-QAM digital modulation techniques.

Keywords: MIMO-FBMC, chaos-based physical layer security, digital precoding, mmwave geometrical channel, SNR.

I. Introduction

In perspective of rapid increase in the number of subscribers of the existing cellular networks (WCDMA/CDMA 2000, HSPA$^+$ aided 3G through LTE-Advanced4G), it is being observed that nearly 50% of the traffic is based on video signal transmission. The commercially deployed 3.9G LTE and 4G LTE-Advanced wireless networks are trying to meet up explosive demand for high quality video through sharing with social media such as YouTube and ultra HD (UHD) and 3D video from mobile devices (e.g., android tablets, smart-phones etc.) [1]. In consideration of exponential growing demand on data rates of our existing wireless networks, we are giving emphasis on the designing and implementation of WWW(Wireless World Wide Web) supportable 5G technology implemented future generation/5G cellular system. The 5G system has not yet been standardized. The 5G mobile communications system is targeted at higher spectrum efficiency. Mobile Internet and IoT (Internet of Things) are the two main market drivers for 5G.There will be a massive number of use cases for Mobile Internet and IoT, such as augmented reality, virtual reality, remote computing, eHealth services, automotive driving and so on. All these use cases can be grouped into three usage scenarios, i.e., eMBB (Enhanced mobile broadband), mMTC (Massive machine type communications) and URLLC (Ultra-reliable and low latency communications)[2] In future 5G wireless networks., various modulation schemes such as Filter-bank Multicarrier(FBMC), Generalized Frequency Division Multiplexing, Bi-orthogonal Frequency Division Multiplexing(BFDM, a generalization of the classical CP-OFDM scheme capable of providing lower intercarrier interference (ICI) and lower ISI)., Universal Filtered Multicarrier (UFMC), Time-frequency Packing(TFP) are being considered for adoption. In FBMC, the transmission bandwidth can be exploited at full capacity using OQAM(Offset-QAM)[3] The Offset-QAM-based filter bank multicarrier (FBMC-OQAM) can be considered as a promising alternative to cyclic prefix-orthogonal frequency division multiplexing (CP-OFDM) for the future generation of wireless communication systems. The FBMC-OQAM provides more robustness to channel dispersion with respect to conventional CP-OFDM. The FBMC-OQAM does not require the use of acyclic prefix (CP) causing an increase in its spectral efficiency [4]

II. Review of Related Works

A significant amount of research is being carried out in different academic institutions and industries on identification of key benefits of FBMC as 5G compatible radio interface technology and its effective implementation. In this paper, a brief idea on the works of few researchers is outlined In 2012, Şahin et. al at [5]reviewed and emphasized the key benefits of filter bank multicarrier (FBMC) technology

Author α ω: Department of Applied Physics and Electronic Engineering, University of Rajshahi, Rajshahi, Bangladesh.
e-mails: jinia4944@gmail.com, enayet_apee@ru.ac.bd
Author σ : Department of Electronics and Telecommunication Engineering, Begum Rokeya University, Rangpur, Bangladesh.
e-mail: joarder@brur.ac.bd
Author ρ: Department of Information and Communication Engineering, Pabna University of Science and Technology, Bangladesh.
e-mail: sarwar.iceru@gmail.com

© 2018 Global Journals

and provided a comparative study of different FBMC prototype filter designs under practical channel environments. In 2014, Schellmannet.almadereviewing work on the waveform design of 4G (based on OFDM) and motivated the need for a redesign for 5G in consideration of rendering unfeasibility of OFDM with the advent of the Internet of Things (IoT) and moving to user-centric processing. The authors designed a new waveform called Universal Filtered Multi-Carrier (UFMC) collecting the advantages FBMC[6]. In 2015 at [7], Taheriet. alargued that channel estimation in FBMC was not a straightforward scheme as used in OFDM systems especially under multiple antenna scenarios. The authors proposed a channel estimation method which employed intrinsic interference pre-cancellation at the transmitter side. The outcome of their work showed that their method needed less pilot overhead as compared to the popular intrinsic approximation methods (IAM) in terms of better BER and MSE performance. At[8] in 2015, Bazziet. al mentioned that Vehicle-to-vehicle (V2V) communications was anticipated as one of key future services imposing challenging requirements on the air interface such as supporting high mobility and asynchronous multiple access. The authors discussed on the design and performance tradeoffs of two 5G targeted waveforms (filter bank multi-carrier with offset quadrature amplitude modulation (FBMC/OQAM) and filtered OFDM (FOFDM) with focusing specifically on V2V communications by utilizing a realistic geometry-based stochastic V2V channel model. They showed that FBMC/OQAM outperformed F-OFDM approaches in some severe V2V scenarios. In 2016 at[9], Weitkemperet.alconducted real hardware experiments to investigate the performance of three waveform families: CP-OFDM, filter bank multicarrier with offset quadrature amplitude modulation (FBMC/OQAM) and universal-filtered OFDM (UF-OFDM). FBMC/OQAM. The outcome of their experimental work ratified that the FBMC/OQAM had the benefit of very low side lobes leading to less inter-carrier interference in asynchronous and high mobility scenarios. At[10] in 2016, Gorganiet. al proposed a high-performance and flexible Peak-to-Average Power Ratio(PAPR) reduction algorithm for FBMC-OQAM signal model and showed that their proposed algorithm had no degradation as compared to OFDM. In 2017 at [11], Lizeagaet.alfocused on the lacking of robustness of the existing IEEE 802.11, IEEE 802.15.1 or IEEE 802.15.4 standard based industrial wireless communications in perspective of real-time requirements for factory automation. The authors analyzed FBMC-OQAM, GFDM-OQAM and WCP-COQAM modulation candidates for 5G in terms of bit error rate, power spectral density and spectral efficiency over highly dispersive channels and assessed the suitability of these modulation systems for industrial wireless communications based on cognitive radio. Additionally, they provided additional details on windowing that affecting the protection against highly dispersive multipath channels and the spectral efficiency in WCP-COQAM. In 2017 at [12], Wang et. al, demonstrated experimentally a digital mobile fronthaul (MFH) architecture using delta-sigma modulation both one-bit and two-bit) as the new digitization interface for transmission of digital signals over on-off keying (OOK) or 4-level pulse-amplitude-modulation (PAM4) optical intensity modulation-direct detection (IM-DD) links. The authors demanded that delta-sigma modulators were supportable of high-order modulations (256QAM/ 1024QAM) and such modulators were 5G compatible with filter-bank-multicarrier (FBMC) signals.

III. Signal Processing and Detection Techniques

In this section, various signal processing and signal detection techniques have been outlined briefly.

a) Massive MIMO Fading Channel Estimation

In estimation of ray path geometry based 16×256 sized mmWave massive MIMO fading channel $\mathbf{H}_{\text{mmwave}}$, it is assumed that the N_t(=256) transmitting and N_r (=16) receiving antennas are arranged in uniform linear array (ULA).Such MIMO channel has limited scattering with Lu (=6) scatterers. Each scatterer is assumed to contribute a single propagation path between the base station (BS) and mobile station (MS). The geometrical channel model $\mathbf{H}_{\text{mmwave}} \in C^{N_r \times N_t}$can be written as:

$$H_{mmwave} = \sqrt{\frac{N_t N_r}{\rho L_u} \sum_{l=1}^{L_u} \alpha_{u,l} a_{MS}(\theta_{u,l}) a^*{}_{BS}(\phi_{u,l})} \quad (1)$$

where, $\alpha_{u,l}$ is the complex gain of the lth path including the path loss, ρ is the path loss between base station (BS) and mobile station (MS). The variable $\theta_{u,l}$ and $\phi_{u,l} \in [0,2\pi]$ are the lth path's angle of arrival and departure (AoAS/AoDs) respectively. Finally, $\mathbf{a}_{\mathbf{BS}}(\phi_{u,l})$ and $\mathbf{a}_{\mathbf{MS}}(\theta_{u,l})$ are the antenna array response vectors of the BS and MS respectively.

© 2018 Global Journals

With available knowledge of the geometry of uniform linear antenna arrays, $a_{BS}(\phi_{u,l})$ is defined as:

$$a_{BS}(\phi_{u,l}) = \frac{1}{\sqrt{N_t}}[1, e^{j\frac{2\pi}{\lambda}d\sin(\phi_{u,l})}, \ldots\ldots\ldots e^{j(N_t-1)\frac{2\pi}{\lambda}d\sin(\phi_{u,l})}]^T \quad (2)$$

and

$$a_{MS}(\theta_{u,l}) = \frac{1}{\sqrt{N_r}}[1, e^{j\frac{2\pi}{\lambda}d\sin(\theta_{u,l})}, \ldots. e^{j(N_r-1)\frac{2\pi}{\lambda}d\sin(\theta_{u,l})}]^T \quad (3)$$

where, λ is the signal wavelength and d is the distance between two consecutive antenna elements.

The massive MIMO mmWave fading channel $\mathbf{H}_{\text{mmwave}}$ is further normalized to get a modified form of fading channel matrix as:

$$\hat{\mathbf{H}} = \mathbf{S} \odot \mathbf{H}_{\text{mmwave}} \quad (4)$$

where, $\odot$ is indicative of Hadamard product, S is the 16×256 sized matrix whose each element is inverse of magnitude of each complex element of $\mathbf{H}_{\text{mmwave}}$. The squared value of the Frobenius norm of the normalized channel matrix $\hat{\mathbf{H}}$ is given by[13, 14]

$$[\|\hat{\mathbf{H}}_F\|^2] = \mathbf{N}_t\mathbf{N}_r \quad (5)$$

b) Digital Precoding

Digital precoding is generally used to control both the phases and amplitudes of the original signals to cancel interferences in advance. In consideration of designing digital precoding for single-user mmWave massive MIMO system, it is assumed that the base station (BS) employs N_t antennas to simultaneously transmit N_r data streams to a user with N_r antennas ($N_r < N_t$). The BS applies an $N_t \times N_r$ digital precoder D and the transmitted signal prior to D/A conversion can be presented by-

$$x = Ds \quad (6)$$

where, s is the $N_r \times 1$ original signal vector before precoding with normalized power as $E(ss^H) = (1/N_r)I_{Nr}$, To meet up the total transmit power, D satisfies

$$\|D\|_F^2 = trace(DD^T) = N_r \quad (7)$$

In terms of geometrical channel presented in Equation (4), the digital precoder is given by[15]

$$D = \sqrt{\frac{N_r}{tr(FF^H)}}F \quad (8)$$

where, $F = \hat{\mathbf{H}}^H$

c) Lattice Reduction(LR) based Zero-forcing(ZF) Detection

In our16×256 simulated system, the received signal in terms of transmitted signal, fading channel H and white Gaussian noise n with a variance σ_n^2 can be written as:

$$Y = \hat{H}Ds = Hs + n \quad (9)$$

where, $H = \hat{H}D$ is the 16×16 sized equivalent channel matrix. In LR based ZF signal detection scheme, the equivalent channel matrix H is considered to be consisted of 16×16 sized lattice reduced orthogonal matrix **G** and a 16×16 sized unimodular matrix **U** such that

$$H = GU \quad (10)$$

The unimodular matrix U is estimated using the following relation:

$$U = \overline{H}H^T \quad (11)$$

where, the matrix $\overline{H}$ is the Moore-Penrose pseudo-inverse of matrix H and $(.)^T$ is indicative of Hermitian transpose in all cases as presented in this paper.
The equation (10) can be rewritten as:

$$U^TG = H^T \quad (12)$$

From equation (12), the orthogonal matrix G can be estimated as:

$$G = (U^T)^{-1}H^T \quad (13)$$

The LR-based ZF signal detection linear filter, W^H can be written in terms of orthogonal matrix **G** as:

$$W^T = (G^TG)^{-1}G^T \quad (14)$$

Equation(9) can be rewritten as

$$Y = GUs + n = Gc + n \quad (15)$$

where, c=Us , Multiplying equation (15) by G^T

$$G^TY = G^TGc + G^Tn \quad (16)$$

Neglecting noise contribution to expected signal from equation (16), we can write:

$$\tilde{c} = (G^TG)^{-1}G^TY = W^TY \quad (17)$$

© 2018 Global Journals

The estimated transmitted signal can be written as:

$$\tilde{s} = U^{-1}\tilde{c} = U^{-1}W^{T}Y \quad (18)$$

d) Lattice Reduction(LR) based ZF-SIC Detection

In LR based Zero-forcing Successive interference cancellation (ZF-SIC) signal detection scheme, the lattice reduced orthogonal matrix **G** is QR factorized as:

$$G=QR \quad (19)$$

where, **Q** is the 16×16 sized unitary and **R** is the 16×16 sized upper triangular matrix . Premultiplying Q^{H} to **Y** in Equation (15), we have

$$Q^{T}Y=Q^{T}Gc+Q^{T}n=Q^{T}QRUs+Q^{T}n=RUs+Q^{T}n=\overline{R}s+Q^{T}n \quad (20)$$

where, $\overline{R}=RU$, neglecting noise contribution to expected signal from equation (20), the estimated transmitted signal can be written as[16,17]:

$$\tilde{\tilde{s}} = (\overline{R}^{T}\overline{R})^{-1}\overline{R}^{T}Q^{T}Y \quad (21)$$

e) Complex-valued LLL(CLLL) Algorithm implemented ZF-SIC Detection

In complex-valued Lenstra–Lenstra–LovKasz (LLL) algorithm implemented ZF-SIC signal detection scheme, the CLLL-reduced orthogonal matrix $\tilde{H}$ is estimated using the CLLL reduction algorithm. In such case, the matrix $\tilde{H}$ is QR factorized as:

$$\tilde{H} = \tilde{Q}\tilde{R} \quad (22)$$

The equation (22) satisfies the following two conditions:

$$|\Re[\tilde{R}_{i,k}]| \le \frac{1}{2}|\Re[\tilde{R}_{i,i}]|, |\Im[\tilde{R}_{i,k}]| \le \frac{1}{2}|\Re[\tilde{R}_{i,i}]|, \forall i < k,$$

$$\delta|\tilde{R}_{i-1,i-1}|^{2} \le |\tilde{R}_{i,i}|^{2} + |\tilde{R}_{i-1,i}|^{2}, \forall i \in [2,N], \quad (23)$$

where, δ is arbitrary chosen from $(\frac{1}{2},1)^{2}$ and $\tilde{R}_{i,k}$ is the (i, k)th entry of $\tilde{R}$.

The detailed pseudo-code of the CLLL algorithm has been presented in Table I. In table 1, $(\alpha)^{*}$ is indicative of complex conjugate value of α. As the equivalent fading channel matrix H 16×16 sized, the value of N considered in Equation(23) is 16 and the value of δ has been considered to 0.75. A comprehensive MATLAB source code for estimating CLLL-reduced orthogonal matrix $\tilde{H}$ and complex-valued unimodular matrix T with assumption of a typically assumed 16×16 sized channel matrix is presented in the Appendix.

© 2018 Global Journals

Table 1: Complex LLL Alogorithm (Using MATLAB Notation)

Input: H; Output: $\tilde{Q}, \tilde{R}$, T

(1) $[\tilde{Q},\tilde{R}]$ = QR Decomposition (H) ;
(2) $\delta \in (\frac{1}{2}, 1)$;
(3) m = size (H , 2) ;
(4) $T=I_m$;
(5) k =2 ;
(6) while $k \leq m$
(7) for n=k-1: -1 : 1
(8) u= round ($(\tilde{R}(n, k) / \tilde{R}(n, n))$) ;
(9) if u ~= 0
(10) $\tilde{R}(1:n, k) = \tilde{R}(1:n, k) - u \cdot \tilde{R}(1:n, n)$;
(11) $T(:, k) = T(:, k) - u \cdot T(:, n)$;
(12) end
(13) end
(14) if $\delta |\tilde{R}(k-1, k-1)|^2 > |\tilde{R}(k, k)|^2 + |\tilde{R}(k-1, k)|^2$
(15) Swap the (k-1)th and kth columns in $\tilde{R}$ and T
(16) $\Theta=\begin{bmatrix} \alpha^* & \beta \\ -\beta & \alpha \end{bmatrix}$ where $\alpha = \frac{\tilde{R}(k-1,k-1)}{||\tilde{R}(k-1:k,k-1)||}$;

$$\beta = \frac{\tilde{R}(k,k-1)}{||\tilde{R}(k-1:k,k-1)||} ;$$

(17) $\tilde{R}(k-1:k, k-1:m) = \Theta \tilde{R}(k-1:k, k-1:m)$;
(18) $\tilde{Q}(:, k-1:k) = \tilde{Q}(:, k-1:k)\Theta^H$;
(19) $k = \max(k-1, 2)$;
(20) *else*
(21) k = k + 1 ;
(22) end
(23) end

The estimated CLLL reduced orthogonal matrix $\tilde{H}$ can be written in terms of estimated complex-valued unimodular matrix T and equivalent fading channel matrix H in different form as[18]:

$$\tilde{H} = HT \quad (24)$$

Equation (24) can be written as:

$$T^T H = \tilde{H}^T \quad (25)$$

From Equation (25),equivalent fading channel matrix H can be written in terms of CLLL reduced orthogonal matrix and complex-valued unimodular matrix as:

$$H = (T^T)^{-1} \tilde{H}^T \quad (26)$$

Equation (9) can be rewritten in case of CLLL algorithm implemented ZF-SIC signal detection scheme as:

$$Y = (T^T)^{-1} \tilde{H}^T s + n = G_1 s + n \quad (27)$$

where, $G_1 = (T^T)^{-1} \tilde{H}^T$, the matrix G_1 is QR factorized as:

$$G_1 = Q_1 R_1 \quad (28)$$

Premultiplying Q_1^H to Yin Equation (27), we have

$$Q_1^T Y = Q_1^T Q_1 R_1 s + Q_1^T n = R_1 s + Q_1 n \quad (29)$$

Neglecting noise contribution to expected signal from equation (29), the estimated transmitted signal can be written as:

$$\tilde{\tilde{s}} = (R_1^T R_1)^{-1} R_1^T Q_1^T Y \quad (30)$$

© 2018 Global Journals

f) Q-Less QR Decomposition Scheme

With Q-less QR Decomposition scheme, the detected signal $\tilde{\mathbf{x}}$ can be found based on the least squares approximate solution to $\tilde{\mathbf{H}} * \tilde{\mathbf{x}} = \tilde{\mathbf{y}}$ where, $\tilde{\mathbf{H}}$ and $\tilde{\mathbf{y}}$ are the channel matrix and received signal respectively. From $\tilde{\mathbf{H}}$ channel matrix, an upper triangular matrix $\tilde{\mathbf{R}}$ of the same dimension as $\tilde{\mathbf{H}}$ is estimated and using the following steps, the detected desired signal $\tilde{\mathbf{x}}$ is computed[19] .

$$\begin{aligned}\tilde{\mathbf{x}} &= \tilde{\mathbf{R}} \setminus (\tilde{\mathbf{R}}^{\mathbf{H}} \setminus (\tilde{\mathbf{H}}^{\mathbf{H}} * \tilde{\mathbf{y}}))\\ \tilde{\mathbf{r}} &= \tilde{\mathbf{y}} - \tilde{\mathbf{H}} * \tilde{\mathbf{x}}\\ \tilde{\mathbf{e}} &= \tilde{\mathbf{R}} \setminus (\tilde{\mathbf{R}}^{\mathbf{H}} \setminus (\tilde{\mathbf{H}}^{\mathbf{H}} * \tilde{\mathbf{r}}))\\ \tilde{\mathbf{x}} &= \tilde{\mathbf{x}} + \tilde{\mathbf{e}}\end{aligned} \quad (31)$$

g) Turbo Channel Coding

In Turbo channel coding technique, two recursive systematic convolutional (RSC) encoders separated by an interleaver are concatenated in parallel. The turbo encoder produces three code bits for every input bit viz., its coding rate is $1/3$. To avoid excessive decoding complexity and code generator polynomials of 13 and 15 in octal numbering system, the turbo channel encoder has a short constraint length of 4 of its RSC encoders. The number of memory elements of each RSC encoder is 3.The turbo encoded binarydata are iteratively decoded using MAP decoding scheme. In such scheme, log likelihood ratio(LLR) for maximizing a posteriori probability (APP) are computed iteratively. In turbo encoding, it is assumed that $\bar{\mathbf{c}} = \mathbf{c}_0, \mathbf{c}_1, \mathbf{c}_2, \mathbf{c}_3 \ldots\ldots\ldots\ldots \mathbf{c}_{N-1}$ is a coded sequence produced by the $1/2$- rated RSC encoder and $\bar{\mathbf{r}} = \mathbf{r}_0, \mathbf{r}_1, \mathbf{r}_2, \mathbf{r}_3 \ldots\ldots\ldots\ldots \mathbf{r}_{N-1}$ is a noisy received sequence where the code-word is $\mathbf{c}_k = \left(\mathbf{c}_k^{(1)}\ \mathbf{c}_k^{(2)}\right)$ with the first bit being the message bit and the second bit being the punctured parity bit. The corresponding received word is

$$\mathbf{r}_k = \left(\mathbf{r}_k^{(1)}\ \mathbf{r}_k^{(2)}\right)$$

The coded bit 0/1 is converted to a value +1/-1. The maximum a posteriori(MAP) decoding is carried out as:

$$\mathbf{c}_k(1) = \left\{\begin{array}{l} +1, \text{if } P(\mathbf{c}_k(1) = +1 \mid \bar{\mathbf{r}}) \geq P(\mathbf{c}_k(1) = -1 \mid \bar{\mathbf{r}}) \\ -1, \text{if } P(\mathbf{c}_k(1) = +1 \mid \bar{\mathbf{r}}) < P(\mathbf{c}_k(1) = -1 \mid \bar{\mathbf{r}}) \end{array}\right\} \quad (32)$$
$$\mathbf{k} = 0,1,2 \ldots\ldots N-1$$

A posteriorilog likelihood ratio(LLR) of $\mathbf{c}_k^{(1)}$ is given by

$$\mathbf{L}\left(\mathbf{c}_k^{(1)}\right) \triangleq \ln\left[\frac{P(\mathbf{c}_k^{(1)} = +1 \mid \bar{\mathbf{r}})}{P(\mathbf{c}_k^{(1)} = -1 \mid \bar{\mathbf{r}})}\right] \quad (33)$$

The MAP decoding rule in Equation (26) can be presented alternatively as:

$$\mathbf{c}_k(1) = \mathbf{sign}\left[\mathbf{L}(\mathbf{c}_k(1) \mid \bar{\mathbf{r}})\right] \quad (34)$$

The magnitude of LLR, $|\mathbf{L}(\mathbf{c}_k(1) \mid \bar{\mathbf{r}})|$ measures the likelihood of $c_k(1) = +1$ or $c_k(1) = -1$. The LLR can be expressed as a function of the probability $\mathbf{P}(\mathbf{c}_k(1) = +1 \mid \bar{\mathbf{r}})$[20,21]

$$\begin{aligned}\mathbf{L}\left(\mathbf{c}_k^{(1)}\right) &= \ln\left[\frac{P(\mathbf{c}_k^{(1)} = +1 \mid \bar{\mathbf{r}})}{P(\mathbf{c}_k^{(1)} = -1 \mid \bar{\mathbf{r}})}\right]\\ &= \ln\left[\frac{P(\mathbf{c}_k^{(1)} = +1 \mid \bar{\mathbf{r}})}{1 - P(\mathbf{c}_k^{(1)} = +1 \mid \bar{\mathbf{r}})}\right]\end{aligned} \quad (35)$$

h) Low-density parity check (LDPC)

Low-density parity check (LDPC)is an emerging new technique that gets even more closer to Shannon rate with long code words. LDPC codes are linear block codes showing good block error correcting capability and linear decoding complexity in time. A (n, k) LDPC encoder operates on an m ×nsizedH_1 matrix where m = n-k. It is low density because the number of 1s in each row $w_r$is « *m* and the number of *1s* in each column $w_c$is « *n*. A LDPC is regular if $w_c$is constant for every column and $w_r = w_c(n/m)$ is also constant for every row. Otherwise it is irregular. In LDPC encoding, the codeword (c_0, c_1, c_2, c_3, …,c_n) consists of the message bits (m_0, m_1, m_2,...,m_k) and some parity check bits and the equations are derived from H_1 matrix in order to generate parity check bits. The solution in solving the parity check equations can be written as:

$$H_1 c^T = 0 \quad (36)$$

© 2018 Global Journals

where such mathematical manipulation can be performed with a generator matrix G_1. G_1 is found from H_1 with Gaussian elimination which can be written as follows:

$$H_1 = [P^T : I] \quad (37)$$

And G_1 is

$$G_1 = [I : P \quad (38)$$

Hence, ccodeword is found for message word *x* as follows $c = xG_1 = [x : xP]$.

The graphical representation for a typical (8, 4) LPDC encoding is shown in Fig. 1. The graphical representation utilizes variable nodes (*v*-nodes) and check nodes (*c*-nodes). The graph has four*c*-nodes and eight*v*-nodes. The check node $f_i$is connected to $c_i$if $h_{ij}$of H_1 is a 1. This is important to understand the decoding. Decoding tries to solve the (n-k) parity check equations of the H_1 matrix. There are several algorithms defined to date and the most common ones are message passing algorithm, belief propagation algorithm and sum–product algorithm [20]. In this paper, we have employed sum-product decoding algorithm as presented in [21].

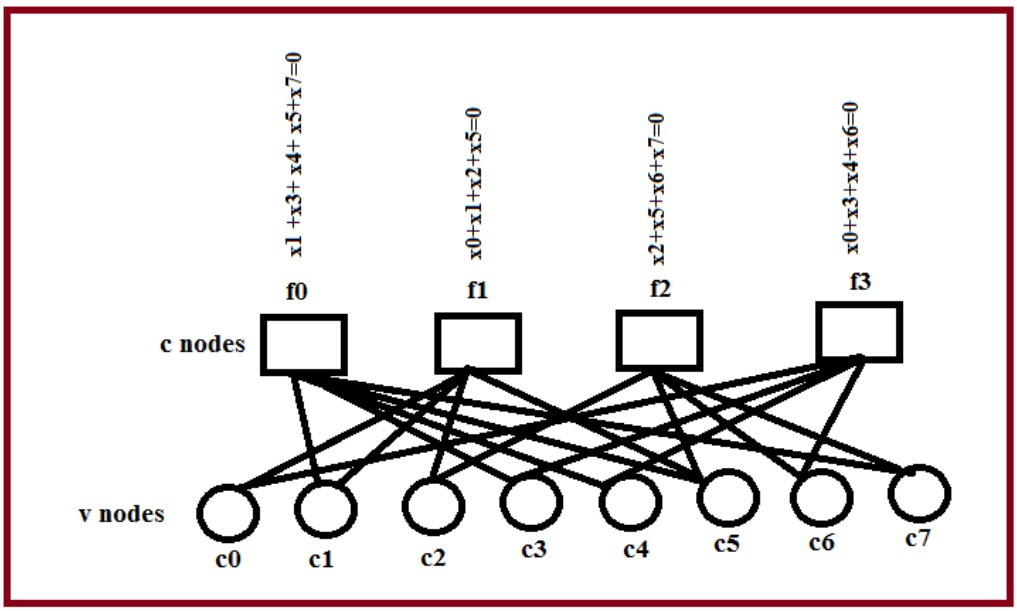

Figure 1: Graphical representation of a (8, 4) LDPC code

i) (3, 2) SPC Channel Coding

In SPC channel coding, the transmitted binary bits are rearranged into very small code words consisting of merely two consecutive bits. In such coding, (3, 2) SPC code is used with addition of a single parity bit to the message u = [u0, u1] so that the elements of the resulting code word x = [x0, x1, x2] are given by x0 = u0, x1 = u1 and x2 = u0 ⊞u1 [22].
where, ⊞ denotes the sum over GF (2)

IV. Audio to Image Conversion Aided Encryption

In audio to image conversion aided chaos-based cryptosystem, Henon, a two-dimensional discrete chaotic map has been used to implement different equations of the Lorenz system as:

$$x_{i+1} = y_{i+1} - \alpha 1\, x_i \quad (39)$$
$$y_{i+1} = \beta 1\, x_i \ .$$

where, initial parameters are $\alpha 1$, $\beta 1$ and the initial point is (x_0, y_0). Each point (x_n, y_n) is mapped to a new point (x_{n+1}, y_{n+1}) through the Henon map under consideration of $\alpha 1 = 1.4, \beta 1 = 0.3$ and $x_0 = y_0 = 0.1$.A segment of considered audio signal has 30,000 samples which on 8-bit A/D conversion provides $100 \times 100 \times 3$ integer values with each value ranging from 0-255. The plain color image is generated from the audio signal and it is $100 \times 100 \times 3$ pixel sized. Both the plain color image and the secret color images are the same in height and width. For processing of each red(R), green(G) and blue(B) components of created plane image, the minimum iterations of Henon map is $m^2 (= 100 \times 100)$.As first few iterations seem fairly close together, therefore, the total number of iterations is $m^2 + 100$ with discarding first 100 points to achieve higher randomness. The 2-D pixel distribution of each R,G,B components of plane image are resized into 10000 pixels. Another auxiliary color image of identical pixel size can be generated using the following relation:

© 2018 Global Journals

$$\begin{aligned} pixXR_i &= abs(\lfloor x_{100+i} \times \gamma 1 \rfloor) \mod 256, \quad i=1,\ldots\ldots,m^2 \\ pixXG_i &= abs(\lfloor x_{100+i} \times \gamma 2 \rfloor) \mod 256, \quad i=1,\ldots\ldots,m^2 \\ pixXB_i &= abs(\lfloor x_{100+i} \times \gamma 3 \rfloor) \mod 256, \quad i=1,\ldots\ldots,m^2 \end{aligned} \tag{40}$$

where, $pixXR_i$, $pixXG_i$ and $pixXB_i$ are the pixel values and $\gamma 1=12345678, \gamma 2=23456789$ and $\gamma 3=34567891$ are the setting values of the R, G and B components of the auxiliary color image respectively.

On reshaping pixel values presented in Equation(34) from 1-D to 2D form, we can write,

$$\begin{aligned} secImgXR &= reshape\ (pixXR, m, m) \\ secImgXG &= reshape\ (pixXG, m, m) \\ secImgXB &= reshape\ (pixXB, m, m) \end{aligned} \tag{41}$$

If $pixR_i$, $pixG_i$ and $pixB_i$ with $i=1,\ldots\ldots,m^2$ are considered to be pixel values of the R, G and B components of the plane color image , we can write,

$$\begin{aligned} secImgR &= reshape\ (pixR, m, m) \\ secImgG &= reshape\ (pixG, m, m) \\ secImgB &= reshape\ (pixB, m, m) \end{aligned} \tag{42}$$

Finally, encrypted image is generated from a combination of selective components of Equation(35) and (36) by performing the bitwise XOR operation on the corresponding pixels as described by Equation(37)[23].

$$\begin{aligned} secImgRenc &= xor(secImgXR, secImgR)\ . \\ secImgGenc &= xor(secImgXG, secImgG)\ . \\ secImgBenc &= xor(secImgXB, secImgB)\ . \end{aligned} \tag{43}$$

V. FBMC Signal Model and Description of Simulated System

We assume that our simulated5G compatible mmWave massive MIMO FBMC system depicted in Figure 2consists of 1024subcarriers with subcarrier spacing 1/T, where T is the interval between the two consecutive digitally modulated complex-valued symbols in time. Each complex-valued digitally modulated symbol is partitioned into its real-valued in phase and quadrature component symbol(sample). The real valued symbol at the frequency-time index (n; m) is denoted by $d_{n,m}$, where nis the frequency/sub channel index and m is the time index. The transmitted signals are organized in the form of FBMC bursts/ transmission frames with each of them is of N×M sized, where M is the number of real symbol slots per each FBMC burst. The mathematical formula describing the transmit signal in discrete form, s[k] for a FBMC burst can be written as:

$$\begin{aligned} s[k] &= \sum_{n=0}^{N-1}\sum_{m=0}^{M-1} \hat{d}_{n,m}\, g_{n,m}[k] \\ &= \sum_{n=0}^{N-1}\sum_{m=0}^{M-1} d_{n,m}\, g[k - m\frac{M_\Delta}{2}].\exp[j(n+m)\frac{\pi}{2}].\exp(j2\pi nN_\Delta(k - m\frac{M_\Delta}{2})] \\ &= \sum_{n=0}^{N-1}\sum_{m=0}^{M-1} d_{n,m}\, g[k - m\frac{M_\Delta}{2}].\exp[j(n+m)\frac{\pi}{2}].\exp(j2\pi nN_\Delta k).\exp(-j2\pi nN_\Delta m\frac{M_\Delta}{2})] \\ &= \sum_{n=0}^{N-1}\sum_{m=0}^{M-1} d_{n,m}\, g[k - m\frac{M_\Delta}{2}].\exp[j(n+m)\frac{\pi}{2}].\exp(j2\pi nN_\Delta k) \end{aligned} \tag{44}$$

where, M_Δ is the time distance between the consecutive pulses (in samples), N_Δ is the frequency distance between the adjacent sample pulses(1/(total number of samples in N subcarriers),viz. $N_\Delta = \frac{1}{N}$ for discrete representationof the signal spectra), k=0,1,2…..NM-1, $g[k - m\frac{M_\Delta}{2}]$is the delayed impulse response of prototype filter, the phase value $\exp(-j2\pi nN_\Delta m\frac{M_\Delta}{2})]$ in s[k] is neglected customarily, the component $\exp[j(n+m)\frac{\pi}{2}]$ gives the value of ±1 for even values of (n+m) and ±j for odd values of (n+m).the component $\exp[j(n+m)\frac{\pi}{2}]$ alternates real and imaginary between adjacent subcarriers and symbols[24]. In Figure2, a segment of audio signal is considered to have been converted into

© 2018 Global Journals

chaos based encrypted RGB color image with 100 pixels in width and 100 pixels in height. The pixel integer values of its respective three Red, Green and Blue components are converted into 8 bits binary form,

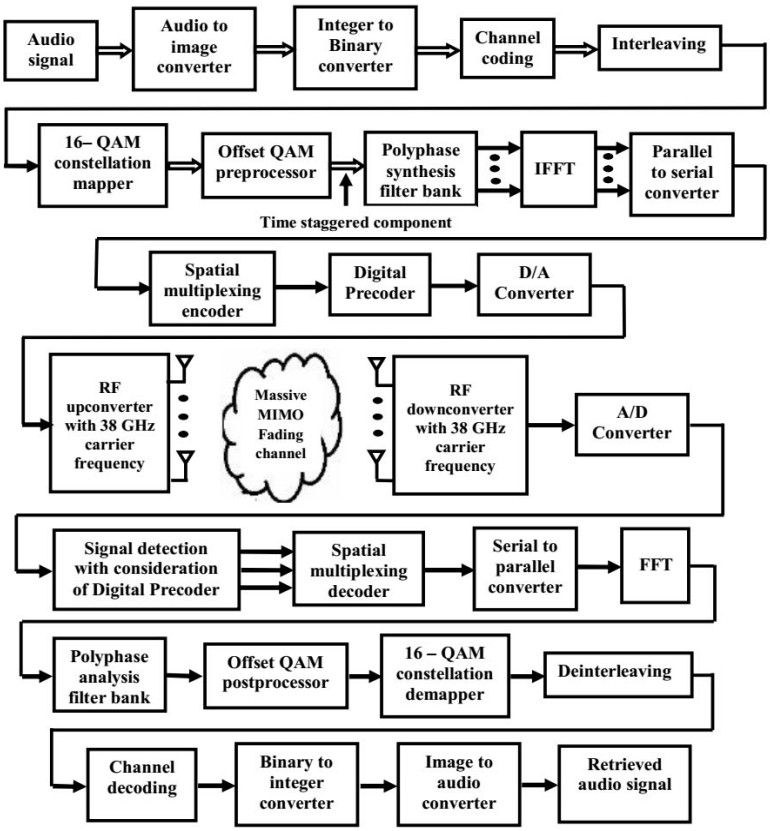

Figure 2: Block diagram of 5G compatible mm Wave massive MIMO FBMC wireless communication system

imaginary parts of each complex-valued symbol are separated to form two new symbols in Offset QAM(OQAM) preprocessing section. The time duration of each Offset QAM symbol is half of the time duration of QAM symbol. In one time index, a FBMC symbol consists of 1024 Offset QAM symbols operated independently on each of the 1024 subcarriers. A low pass prototype filter of coefficient length 4096 is considered with overlapping factor of 4 and it spans four FBMC symbols. The low pass prototype filter is decomposed into 1024 band pass polyphase filters assigned for each subcarrier with each sub and polyphase filter consisting of four real valued filter coefficients. Prior to multicarrier modulation in IFFT section, each FBMC symbol consisting of 1024 Offset QAM symbols are synthesized with polyphase synthesis filter bank. The filtered signals are parallel to serially converted and fed into spatial multiplexing encoder and eventually they are fed into digital precoder. Then the digitally precoded data streams are RF up converted with 38 GHz carrier frequency and transmitted from each of the transmitted antennas through massive MIMO fading channel. In receiving section, the transmitted signals are RF down converted and subsequently processed for signal detection based on considered previously designed digital precoder at the transmitter. The detected signal are subsequently processed in spatial multiplexing decoder, serial to parallel converter, multicarrier demodulation in FFT section and filtered in polyphase analysis filter bank. In Offset QAM post processing section, the in phase and quadrature components are combined and digitally demodulated/demapped, de interleaved, channel decoded, binary to integer converted, decrypted and eventually transmitted audio signal is retrieved.

VI. Result and Discussion

In this section, simulation results using MATLAB R2017 are presented to illustrate the significant impact of various types of signal detection and channel coding techniques on performance evaluation of a single-user digitally precoded5G compatible mmWave massive MIMO FBMC system in terms of bit error rate (BER) on encrypted audio signal transmission. It has been assumed that the channel state information (CSI) of the geometrically estimated mmWave large MIMO fading channel is available at the receiver and the fading channel coefficients are constant during simulation. The proposed model is simulated to evaluate the system performance with considering the following parameters presented in the Table 2.

© 2018 Global Journals

Table 2: Simulation Parameters

Data Type	Audio Signal
No of samples	30,000
Sampling frequency of audio signal	48KHz
Carrier frequency	28GHz
Encryption technique	Audio to image(size: 100×100×3 pixels)
Path loss constant	3
Path loss, dB for carrier frequency wavelength λ and transmitter-receiver distance , d	$-20\log_{10}(\lambda/4\pi d)$
No of iteration used in LDPC decoding	10
Antenna configuration	32 x 256 Large MIMO Channel
Channel Coding	LDPC, Turbo and (3,2)SPC
LDPC Channel decoding	Log-domain sum product
Digital Modulation	16-QAM
Signal Detection Scheme	LR based linear detection, LR based ZF-SIC, CLLL based LR and Q-Less QR
SNR	0 to 10 dB
Channel	AWGN and Rayleigh

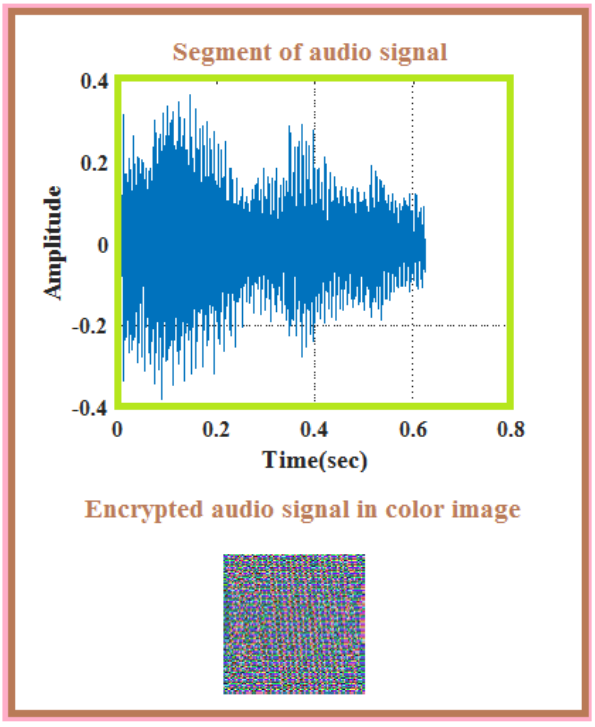

Figure 3: Conceptual graphical illustration showing the encryption of audio signal in non-understandable color image

Figure3 shows a segment of audio signal and the encryption of audio signal in non-understandable color image with 16-QAM digital modulation.

© 2018 Global Journals

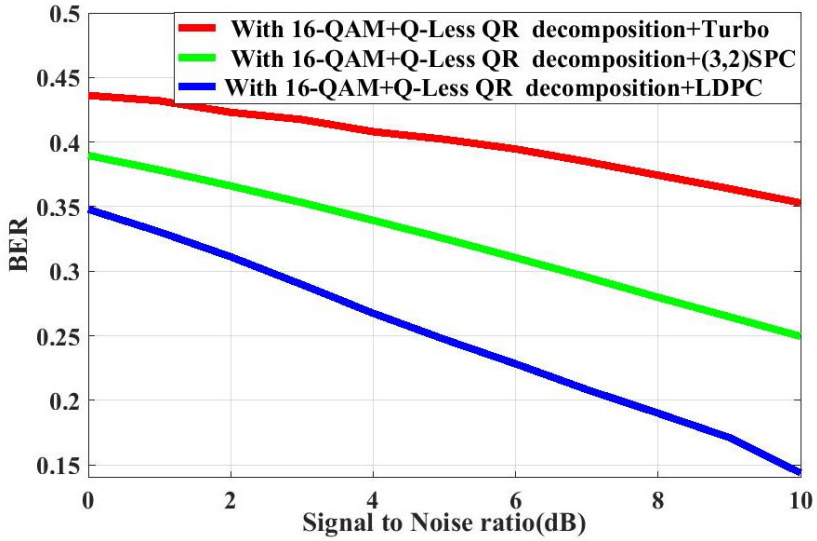

Figure 4: BER performance of secured5G compatible mmWave massive MIMO FBMC system with implementation of Q-Less QR signal detection, 16-QAM digital modulation and various channel coding schemes

The graphical illustrations presented in Figure 4 through Figure 7 manifest that the performance of the simulated system in terms of Bit error rate (BER) Vs. Signal to noise ratio(SNR) values at different scenario is clearly understandable and well defined. It is noticeable in Figure 4 that under consideration of implemented Q-Less QR signal detection technique, the estimated BER values are 0.4230, 0.366 and 0.3111 in case of Turbo, (3,2) SPC and LDPC channel coding schemes respectively for a typically assumed SNR value of 2 dB. In such specifically considered SNR value, system performance improvement of 1.330 dB and 0.706 dB are achieved in LDPC as compared to Turbo and (3,2) SPC channel coding techniques.

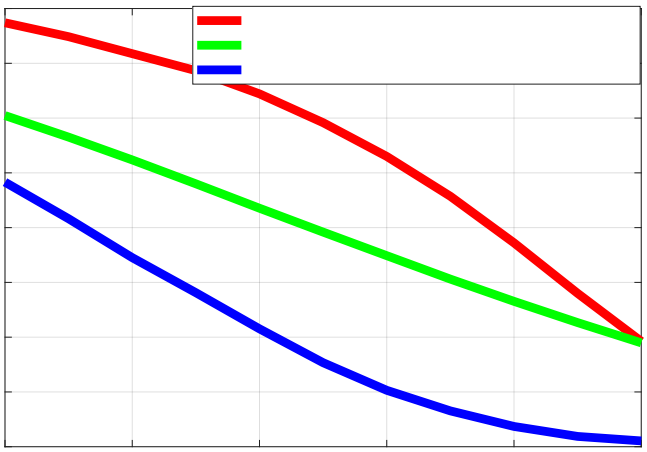

Figure 5: BER performance of secured 5G compatible mmWave massive MIMO FBMC system with implementation of CLLL aided Lattice Reduction signal detection, 16-QAM digital modulation and various channel coding schemes

Figure 5 show the impact of implementing CLLL aided Lattice Reduction signal detection technique on system performance. In such case, it is quite observable that at SNR value of 2dB,the estimated BERs are found to have values of 0.3588, 0.2618 and 0.1635 in case of Turbo, (3, 2) SPC and LDPC channel coding schemes respectively which are indicative of system performance improvement of 3.413 dB and 2.044 dB in LDPC as compared to Turbo and (3, 2) SPC channel coding techniques. At 20% BER, SNR gain of 6.7 dB and 3.9 dB are obtained in LDPC as compared to Turbo and (3, 2) SPC channel coding techniques.

© 2018 Global Journals

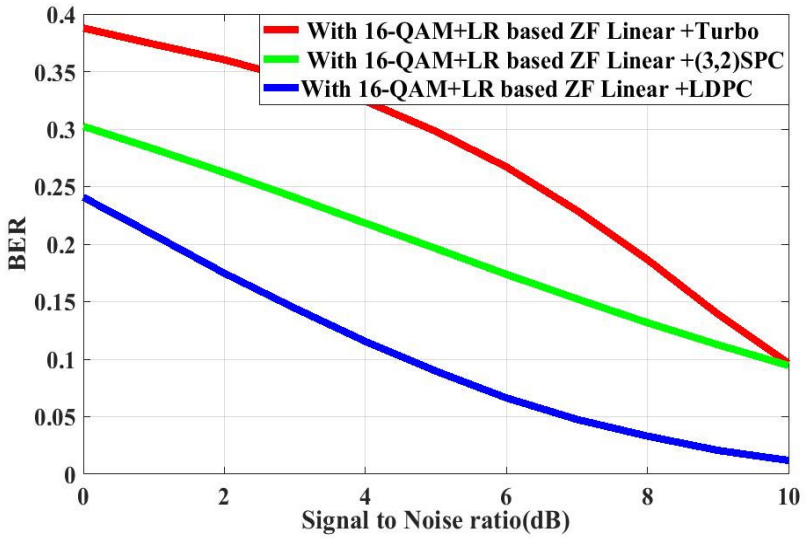

Figure 6: BER performance of secured 5G compatible mmWave massive MIMO FBMC system with implementation of LR based ZF linear signal detection, 16-QAM digital modulation and various channel coding schemes.

For identical consideration of SNR value(2dB) under scenario of LR based ZF linear signal detection, it is seen from Figure 6 that the estimated BER values are 0.3603, 0.2622 and 0.1747 in case of Turbo, (3,2) SPC and LDPC channel coding schemes respectively which ratify system performance improvement of 3.144 dB and 1.763 dB in LDPC as compared to Turbo and (3,2) SPC channel coding techniques. At 20% BER, SNR gain of 6.4 dB and 3.6 dB are obtained in LDPC as compared to Turbo and (3,2) SPC channel coding techniques.

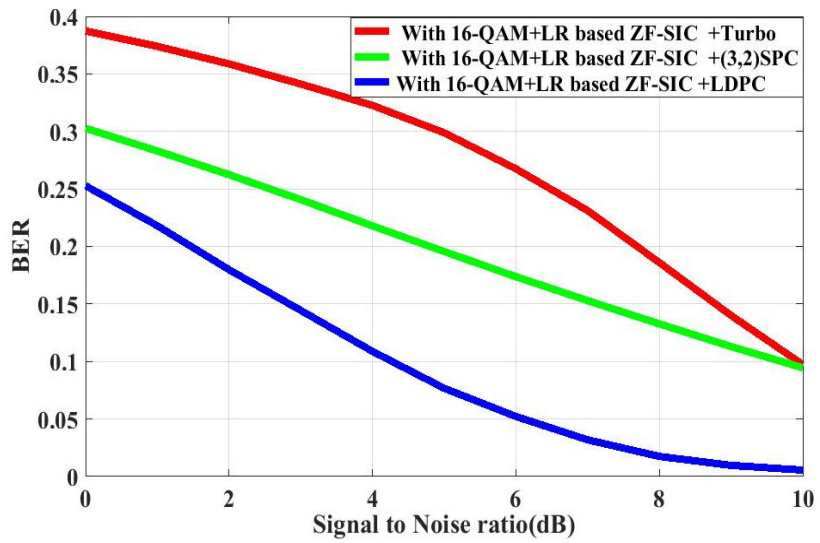

Figure 7: BER performance of secured 5G compatible mmWave massive MIMO FBMC system with implementation of LR based ZF-SIC signal detection, 16-QAM digital modulation and various channel coding schemes

Figure 7 represents characteristics features of the simulated system under implementation of LR based ZF-SIC signal detection technique. With previously considered SNR value, the estimated BER values are 0.3587, 0.2624 and 0.1798 in case of Turbo, (3,2) SPC and LDPC channel coding schemes respectively. In such situation, system performance improvement of 2.999 dB and 1.642 dB are achieved in LDPC as compared to Turbo and (3,2) SPC channel coding techniques. At 20% BER, SNR gain of 6.2 dB and 3.4 dB are obtained in LDPC as compared to Turbo and (3, 2) SPC channel coding techniques.

VII. Conclusions

In this paper, the performance of single-user digitally precoded mmWave massive MIMO FBMC wireless communication system has been investigated on encrypted audio signal transmission under utilization of various modern channel coding and signal detection techniques. From the simulation results, it can be

© 2018 Global Journals

concluded that the presently considered single-user digitally precoded mmWave massive MIMO FBMC wireless communication system shows satisfactory performance with lower order digital modulation under implementation of Lattice Reduction(LR) based ZF-SIC signal detection and LDPC Channel coding technique.

Appendix

```
clear all;
close all;
H=(1/sqrt(2)).*[randn(16,16)+sqrt(-1)*randn(16,16)];%16×16 sized channel matrix
[Q,R] = qr(H);
delta= 0.75;
% T is unimodular matrix
T=diag(ones(1,16));%Initialization with consideration of 16×16 sized identity matrix
m = size(H, 2); %  m=16
rho = 2;
while rho <=m
for l = 1 :rho-1
mu = round((R(rho-l, rho)/R(rho-l, rho-l)));
if mu ~= 0
R(1:rho-l,rho)=R(1:rho-l,rho)-mu*R(1:rho-l,rho-l);
T(:, rho)= T(:,rho)-mu*T(:, rho-l);
end
end
%%%%%%%%%%%%%%%%%%%%%%%%%%%%%
first_term=delta*abs(R(rho-1,rho-1).^2);
second_term=abs(R(rho-1,rho).^2)+abs(R(rho,rho).^2);
if(first_term > second_term)
%Swap the (k-1) th and k th columns in R and T
bb=R(:,rho);
R(:,rho)=R(:,rho-1);
R(:,rho-1)=bb;
cc=T(:,rho);
T(:,rho)=T(:,rho-1);
T(:,rho-1)=cc;
alpha=(R(rho-1,rho-1))/normest(R(rho-1:rho,rho-1));
beta=(R(rho,rho-1))/normest(R(rho-1:rho,rho-1));
thetacut=[conj(alpha) beta ;-beta alpha];
R(rho-1:rho,rho-1:m) =thetacut*R(rho-1:rho,rho-1:m);
Q(:,rho-1: rho) = Q(:, rho-1:rho)*thetacut';
rho = max(rho-1,2);
else
rho=rho+1;
end
end
%%%%%%%%%%%%%%%%%%%%%%%%%%%%%
Htilt=Q*R;% CLLL-reduced orthogonal matrix , Equation(22)
%T is the complex-valued  unimodular matrix
%Verification of Equation (24)
```


© 2018 Global Journals

```
Htilt1=H*T;
%%%%%%%%%%%%%%%%%
Htilt(1:5,1:5)
Htilt1(1:5,1:5)
%%%%%%%%%%%%%%%%%%%%%%%%
```

References Références Referencias

1. T. S. Rappaport, S. Sun, R. Mayzus, H. Zhao, Y. Azar, K. Wang, G. N. Wong, J. K. Schulz, M. K. Samimi, F. Gutierrez, 2013: Millimeter wave mobile communications for 5G cellular: It will work!, IEEE Access, vol. 1, pp. 335-349.
2. Wei Xiang, Kan Zheng and Xuemin (Sherman) Shen, 2017: 5G Mobile Communications, Springer International Publishing Company, Switzerland.
3. Fa-Long Luo and Charlie (Jianzhong) Zhang, 2016: Signal Processing for 5G Algorithms and Implementations, John Wiley & Sons, Ltd, United Kingdom.
4. François Rottenberg, Xavier Mestre, Dmitry Petrov, François Horlin and Jérôme Louveaux, 2017: Parallel Equalization Structure for MIMO FBMC-OQAM Systems under Strong Time and Frequency Selectivity, IEEE Transactions on Signal Processing, vol.65, no.17, pp. 4454 – 4467.
5. AlphanŞahin; İsmail Güvenç; Hüseyin Arslan, 2013: A comparative study of FBMC prototype filters in doubly dispersive channels, IEEE Globecom Workshop, pp. 197 – 203.
6. Malte Schellmann, Zhao Zhao, Hao Lin, Pierre Siohan, Nandana Rajatheva, Volker Luecken, and Aamir Ishaque, 2014: FBMC-based air interface for 5G mobile: Challenges and proposed solutions, 9th IEEE International Conference on Cognitive Radio Oriented Wireless Networks and Communications (CROWNCOM), pp. 102 – 107.
7. Sohail Taheri, Mir Ghoraishi and Pei Xiao, 2015: Overhead reduced preamble-based channel estimation for MIMO-FBMC systems, IEEE International Wireless Communications and Mobile Computing Conference (IWCMC), pp. 1435 – 1439.
8. Jamal Bazzi, Katsutoshi Kusume, Petra Weitkemper, Keisuke Saito, Anass Benjebbour, Yoshihisa Kishiyama, 2015: Performance of multi-carrier waveforms in vehicle-to-vehicle communications, IEEE Vehicular Networking Conference (VNC), pp. 9 – 16
9. Petra Weitkemper, Johannes Koppenborg, Jamal Bazzi, Rupert Rheinschmitt, KatsutoshiKusume, DraganSamardzija, Rolf Fuchs and Anass Benjebbour, 2016: Hardware experiments on multi-carrier waveforms for 5G, IEEE Wireless Communications and Networking Conference (WCNC), pp. 270 – 275.
10. Saeed Afrasiabi-Gorgani and Gerhard Wunder, 2016: A Versatile PAPR Reduction Algorithm for 5G Waveforms with Guaranteed Performance, 20th IEEE International ITG Workshop on Smart Antennas (WSA 2016), pp.1-7
11. Aitor Lizeaga, Mikel Mendicute, Pedro Manuel Rodríguez and Iñaki Val, 2017: Evaluation of WCP-COQAM, GFDM-OQAM and FBMC-OQAM for industrial wireless communications with Cognitive Radio, IEEE International Workshop of Electronics, Control, Measurement, Signals and their Application to Mechatronics (ECMSM), pp.1-6.
12. Jing Wang, Zhenhua Yu, Kai Ying, Junwen Zhang, Feng Lu, Mu Xu, Lin Cheng, Xiaoli Ma and Gee-Kung Chang, 2017: Digital mobile fronthaul based on delta-sigma modulation for 32 LTE carrier aggregation and FBMC signals, IEEE/OSA Journal of Optical Communications and Networking, vol.9, no.2, pp: A233 - A244.
13. Ahmed Alkhateeb, Omar El Ayach, Geert Leus, and Robert W. Heath Jr, 2013: Hybrid Precoding for Millimeter Wave Cellular Systems with Partial Channel Knowledge, IEEE workshop on Information Theory and Applications (ITA), pp.1-5.
14. Weiheng Ni, Xiaodai Dong and Wu-Sheng Lu, 2015: Near-Optimal Hybrid Processing for Massive MIMO Systems via Matrix Decomposition, Cornell University Library pp.1-9, http://arxiv.org/abs/1504.03777
15. Shahid Mumtaz, Jonathan Rodriguez and Linglong Dai, 2017: mmWave Massive MIMO A Paradigm for 5G, Academic Press, an imprint of Elsevier Inc, United kingdom.
16. Lin Bai and Jinho Choi, 2012: Low Complexity MIMO Detection, Springer-Verlag New York, USA.
17. Ying Hung Gan, Cong Ling, and Wai Ho Mow, 2006: Complex Lattice Reduction Algorithm for Low-Complexity MIMO Detection, pp.1-9, https://arxiv.org/pdf/cs/0607078.pdf
18. Xiaoli Ma, and Wei Zhang, 2008: Performance Analysis for MIMO Systems with Lattice-Reduction Aided Linear Equalization, IEEE Transactions on Communications, vol. 56, no. 2.
19. Steven T. Karris, 2004: Numerical Analysis Using MATLAB and Spreadsheets, Second Edition, Orchard Publications, California, USA.
20. Mustafa Ergen, 2009: Mobile Broadband including WiMAX and LTE, Springer US, USA.

© 2018 Global Journals

21. H. Futaki, and T. Ohtsuki, 2002: Low-Density Parity-Check (LDPC) Coded OFDM systems, IEEE International Conference on Communications, New York, USA.
22. Giorgio M. Vitetta, Desmond P. Taylor, Giulio Colavolpe, Fabrizio Pancaldi and Philippa A. Martin, 2013: Wireless Communications Algorithmic Techniques, John Wiley and Sons Ltd, United Kingdom.
23. Ali Soleymani, Md Jan Nordin, and Elankovan Sundararajan, 2014: A Chaotic Cryptosystem for Images Based on Henon and Arnold Cat Map, Hindawi Publishing Corporation, The Scientific World Journal, vol. 2014, Article ID 536930.
24. Hanna Bogucka, Adrian Kliks and Paŵe Kryszkiewicz, 2017: Advanced Multicarrier Technologies for Future Radio Communication 5G and Beyond, John Wiley & Sons, Inc, USA.

© 2018 Global Journals